Proceedings of the 2001 IEEE/RSJ
International Conference on Intelligent Robots and Systems
Maui, Hawaii, USA, Oct. 29 – Nov. 03, 2001

Manipulability and Force Ellipsoids for Continuum Robot Manipulators

Ian A. Gravagne and Ian D. Walker
Clemson University, Dept. of Electrical and Computer Engineering
igravag@ces.clemson.edu and ianw@ces.clemson.edu

Abstract

Manipulability and force ellipsoids have long been a useful tool for analyzing the relative capabilities of robotic manipulators to move in, or to exert forces in, certain directions. The purpose of this paper is to first formulate, and then to examine, the manipulability and force ellipsoids for continuum robots. Continuum robots have continuously flexible backbones; consequently, their infinite-dimensional kinematics present special challenges in the formulation and interpretation of ellipsoids.

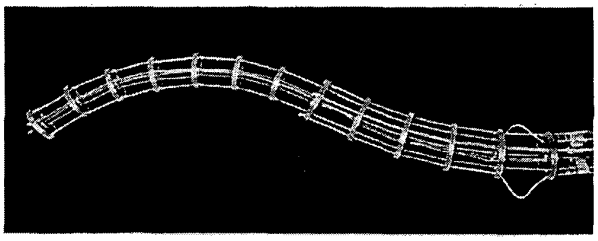

Figure 1: The Tentacle Manipulator in planar configuration.

1 Introduction

The study of continuum robotics is driven by the observation that, in nature, octopus tentacles, elephant trunks and snakes can manipulate their environments with incredible agility and maneuverability. The fields of hyper-redundant, high-degree-of-freedom (HDOF) and continuum robots all seek to reproduce the characteristics and trunks and tentacles to some extent by endowing manipulators with far more degrees of freedom than are absolutely necessary to position and orient their end-effectors. However, unlike hyper-redundant and HDOF manipulators, continuum robots feature "backbones" that are continuously and elastically flexible. They may be redundantly or even hyper-redundantly actuated, but do not have to be. Because their actuation schemes are necessarily finite-dimensional, yet their kinematics are infinite-dimensional, they possess a unique attribute we term "inherent compliance". That is, the shape of the robot not only conforms to the constraints applied by the actuators, but also to external forces exerted by the environment (by obstacles, for instance). Though continuum robots will likely never be able to match the positioning precision of traditional rigid-link robots, they may prove exceptionally useful in such areas as endoscopy development, exploration for hazardous, delicate or unknown environments, and nano-manipulation, where it is difficult to build joints and stiff links.

The Clemson Tentacle Manipulator is a prototype continuum manipulator, seen in figure 1. Its backbone is a highly elastic rod, forced into certain configurations by the periodic application of moments along the backbone length. The forces that generate the moments are transmitted via cables up the backbone to a remote actuator bay, making the manipulator itself very lightweight and of relatively simple design. Though the Tentacle Manipulator is a three-dimensional device, we focus in this paper on its planar equivalent, which has a simple piece of spring-steel as the backbone. The objective of this paper is to examine the ability of a planar continuum robot's end-effector to move in response to given actuator velocities, and to exert forces in response to given actuator torques.

The ellipsoid provides the standard tool for studying a manipulator's velocity and static force characteristics, and a large volume of work discussing ellipsoids exists in the literature. For a good overview see [9]. For background into the kinematics and path-planning of continuum and hyper-redundant robots, see [1]-[7] and [8]. The term "continuum" first appears in the survey paper [10]. Also, [4] and [5] discuss the dynamics of continuum planar robots, and in fact we take the dynamic model in [5] as a starting point in this paper.

2 Background

Before discussing the details of continuum kinematics, we briefly review the theory of manipulability and force ellipsoids for standard manipulators. Pictured in figure 2 is a planar, 3-link robot. We are interested in what happens at its end-effector, located at the position $\underline{x}_{ee} = \begin{bmatrix} x_{1,ee} & x_{2,ee} \end{bmatrix}^T$. The forward kinematics provide the mapping between the actuator joint angles, θ_i, and

0-7803-6612-3/01/$10.00©2001 IEEE

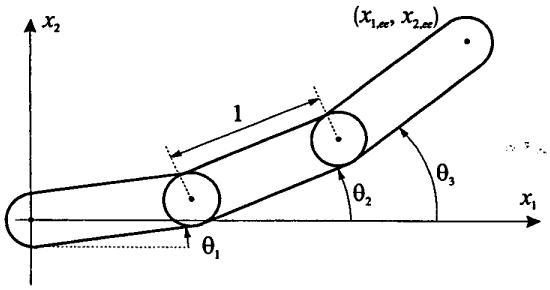

Figure 2: A simple 3-link planar manipulator.

$\underline{x}_{ee}$ as

$$\underline{x}_{ee} = \underline{f}(\underline{\theta}); \qquad \underline{\theta} = \begin{bmatrix} \theta_1 & \theta_2 & \theta_3 \end{bmatrix}. \tag{1}$$

If the joint angles have a given velocity, then the velocity of the end-effector is linearly related to the velocities of the joints, so that

$$\dot{\underline{x}}_{ee} = J(\underline{\theta})\dot{\underline{\theta}}; \qquad J \triangleq \frac{\partial \underline{f}(\underline{\theta})}{\partial \underline{\theta}} \tag{2}$$

where J is the manipulator Jacobian. In the case of our example 3-link robot, we find that

$$J = \begin{bmatrix} -s_{\theta_1} & -s_{\theta_2} & -s_{\theta_3} \\ c_{\theta_1} & c_{\theta_2} & c_{\theta_3} \end{bmatrix} \tag{3}$$

where $s_{\theta_i} \triangleq sin(\theta_i)$ and $c_{\theta_i} \triangleq cos(\theta_i)$.

One might ask the question, what is the set of all $\dot{\underline{x}}_{ee}$ such that $\dot{\underline{\theta}}$ has unit norm? Mathematically, this set is called the "manipulability ellipsoid" (or ME), taking the form

$$ME = \left\{ \dot{\underline{x}}_{ee} : \left\| \dot{\underline{\theta}} \right\|^2 = \dot{\underline{\theta}}^T \dot{\underline{\theta}} = 1 \right\} \tag{4}$$

where we have used the fact that, if a norm equals unity, its square also does. Without demonstration, the relationship (2) allows us to rewrite the ME as

$$ME = \left\{ \dot{\underline{x}}_{ee} : \dot{\underline{x}}_{ee}^T J^{+T} J^{+} \dot{\underline{x}}_{ee} = 1 \right\}. \tag{5}$$

The term J^+ is the "pseudoinverse" of the Jacobian. (Interestingly, the ME can be defined using a pseudoinverse regardless of the fact that an infinite number of generalized inverses exist which map from the end-effector velocity to the joint velocity.) For our purposes we use the unweighted pseudoinverse definition,

$$J^+ = J^T (JJ^T)^{-1}, \tag{6}$$

assuming that the manipulator is not in a singular configuration. Given this definition, we find that the ME simplifies to

$$ME = \left\{ \dot{\underline{x}}_{ee} : \dot{\underline{x}}_{ee}^T \left(JJ^T\right)^{-1} \dot{\underline{x}}_{ee} = 1 \right\}. \tag{7}$$

Consequently, the ME will have principal axes in the directions $\underline{v}_i$, with magnitudes $\sqrt{\lambda_i}$, where $\underline{v}_i$ and λ_i are the eigenvectors and eigenvalues of JJ^T. Note that, while the definition of the ME contains an inverse, the practical result is an ellipsoid defined with quantities $\underline{v}_i$ and λ_i which always exist even if the robot is in a singular configuration.

The other ellipsoid of primary interest is the "force ellipsoid" (FE). The FE is the set of all end-effector generalized forces $\underline{f}$ which the robot can exert given that the vector of joint torques $\underline{\tau}$ has unit norm, i.e.

$$FE = \left\{ \underline{f} : \|\underline{\tau}\| = 1 \right\} \tag{8}$$

Fortunately the relationship $\underline{\tau} = J^T \underline{f}$ does not have to be "inverted", so the result follows directly that

$$FE = \left\{ \underline{f} : \underline{f}^T \left(JJ^T\right) \underline{f} = 1 \right\}. \tag{9}$$

Thus, the FE will have principal axes in the directions of $\underline{v}_i$ with magnitudes $\frac{1}{\sqrt{\lambda_i}}$. In effect, the FE is "perpendicular" to the ME, so that the directions in which the robot can exert the greatest force are also the directions in which it is least sensitive to changes in the joint angles. This is an intuitive result, and the ME and FE have been extensively studied and employed to optimize the configuration of robots needing to achieve specific tasks, like resisting an end-effector tool force in a particular direction.

3 Continuum Manipulator Kinematics

The kinematics of a continuum robot depend not only upon geometric constraints, but also upon physical properties of the robot's backbone. In essence, continuum kinematics reflect the robot's minimum potential energy equilibrium. So, in addition to the physical measurements of the robot backbone, we need Young's modulus E for the backbone material, the cross-sectional moment of inertia I, and the shear modulus G. Given a cross-sectional area A for the backbone, the quantities EI, EA, and GA are the bending stiffness, the axial stiffness and the shear stiffness, respectively. Now the position of the backbone is parameterized as a continuous function, $\underline{x}(s)$, and the angle of the backbone is $\theta(s)$. We detail the derivation of the backbone dynamics in [5], along with the appropriate assumptions and simplifications. Here, we simply cancel the time-dependent terms from the dynamics of [5] and find that the kinematics for the backbone are

$$EI\theta'' + \underline{x}'^T TQCQ^T(\underline{x}' - \underline{q}) + m = 0 \tag{10a}$$

$$\left[QCQ^T(\underline{x}' - \underline{q})\right]' = \underline{0} \tag{10b}$$

where the primes denote differentiation with respect to the parameterization variable, $s \in [0, L]$, and L is the

length of the backbone at zero potential energy. The quantity $m(s)$ is the moment density (moment per unit length) applied to the backbone. Also,

$$Q = \begin{bmatrix} c_\theta & -s_\theta \\ s_\theta & c_\theta \end{bmatrix}; \quad T = \begin{bmatrix} 0 & 1 \\ -1 & 0 \end{bmatrix}; \quad (11)$$
$$\underline{q} = \begin{bmatrix} c_\theta \\ s_\theta \end{bmatrix}; \quad C = \begin{bmatrix} EA & 0 \\ 0 & GA \end{bmatrix}.$$

The boundary conditions for the kinematic equations are

$$\theta(0) = 0 \quad (12a)$$
$$\underline{x}(0) = \underline{0} \quad (12b)$$
$$EI\theta'(L) = 0 \quad (12c)$$
$$QCQ^T(\underline{x}' - \underline{q})|_L = \underline{f}. \quad (12d)$$

The backbone's shape changes in response to moments applied at various points along its length, including at $s = L$. Cable tensions, applied through moment arms attached to the backbone, supply these moments. From the actuators, the cables pass through standoffs until they reach their terminal moment arm. Consequently, the cables exert shear forces at every standoff location. The effect of these shear forces is an interesting subject in its own right, but given a sufficient number of standoffs, along with characteristically high stiffness EA and GA, the shear forces contribute little to the overall deformation of the backbone. They are therefore neglected, and only the moments produced at the cable termination points are considered. In past work, when considering only one section (a backbone with only one cable termination point), we accounted for this moment in the boundary term (12c), e.g. $EI\theta'(L) = \tau$. In moving to a situation where there are multiple moment application points along the backbone length, we now choose to incorporate these moments into the field equation (10a), rather than treating each section individually and trying to "glue" the sections together by enforcing continuity of the boundary conditions. Both methods yield the same result, but we seek the method that is easiest to use and manipulate. Given this argument, the distributed moment of (10a) will consist of a sum of Dirac delta distributions. Where a moment τ_i is applied at location s_i, we find

$$m(s) = \sum_{i=1}^{n} \tau_i \delta(s - s_i); \qquad 0 < s_1 < ... < s_n = L. \quad (13)$$

Note that (12c) does not actually imply that the end-effector moment is zero; rather, it is an algorithmic "trick" to allow the introduction of the backbone moments through the moment density function.

We may integrate (10b) and use the boundary axial/shear condition (12d) to deduce that

$$QCQ^T(\underline{x}' - \underline{q}) = \underline{f} \quad (14)$$

which further implies that

$$\underline{x}' = \underline{q} + QC^{-1}Q^T\underline{f}. \quad (15)$$

As a consequence of large EA and GA, (15) suggests that $\underline{x}' \simeq \underline{q}$ and so $\|\underline{x}'\| = 1$, that is, the backbone is essentially inextensible. As an added benefit of this simplification, the parameterization variable s is now simply the arc length of the backbone.

We may also simplify (10a) using boundary condition (12d) to see that

$$EI\theta'' + \underline{x}'^T T\underline{f} + m = 0 \quad (16)$$

and, if no end-effector forces are applied or exerted ($\underline{f} = \underline{0}$), then the robot exhibits constant curvature behavior, i.e.

$$EI\theta'' + m = 0 \quad (17)$$

so that each section takes a semi-circular shape. We have illustrated this phenomenon before in [2]-[3]. In general, we can integrate (16) from s to L to yield

$$EI\theta'(s) = [\underline{x}(L) - \underline{x}(s)]^T T\underline{f} + \sum_{i=1}^{n} \tau_i (1 - u(s - s_i)) \quad (18)$$

where $u(s)$ is the Heaviside step function. This expression simply states that the internal backbone moment at any point s must balance the sum of the applied moments and the moment exerted by end-effector force $\underline{f}$ acting through distance $\underline{x}(L) - \underline{x}(s)$. (The product $[\underline{x}(L) - \underline{x}(s)]T\underline{f}$ is analogous to the cross product $[\underline{x}(L) - \underline{x}(s)] \times \underline{f}$, only in two dimensions.)

4 Global Manipulability Ellipsoid

Given that the angle for a continuum backbone is now a continuous function of arc length, its norm takes an integral form and we define the global manipulability ellipsoid (GME) as

$$GME = \left\{ \dot{\underline{x}}(L) : \left\| \dot{\theta}(s) \right\| = 1 \right\}, \quad (19)$$

where

$$\left\| \dot{\theta}(s) \right\|^2 = \int_0^L \dot{\theta}(s)^2 ds. \quad (20)$$

The set above is termed "global" because it employs the infinite-dimensional functional norm of $\dot{\theta}$, accounting for all possible changes in the backbone angle, even changes not physically achievable by the (finite number of) actuators exerting moments on the backbone. Angle $\theta(s)$ has a solution derived from (18), so we decompose the solution into an infinite sum of orthonormal modal basis functions,

$$\theta(s) = \sum_{i=1}^{\infty} a_i \Phi_i(s) = \underline{a}^T \underline{\Phi}(s) \quad (21)$$

where the "vectors" $\underline{a}$ and $\underline{\Phi}$ are "infinitely" long. The functions $\Phi_i(s)$ can represent any orthonormal basis set here (for instance, in [2] we discuss the use of wavelet basis sets), as long as

$$a_i = \int_0^L \Phi_i(s)\theta(s)ds, \quad \int_0^L \Phi_i(s)\Phi_j(s)ds = \delta_{ij}. \quad (22)$$

Given that $\underline{x}(L) = \int_0^L \underline{q}(\theta(s))ds$, use of the chain rule with reference to (11) yields the time derivative of $\underline{x}(L)$,

$$\dot{\underline{x}}(L) = \int_0^L \frac{\partial \underline{q}}{\partial \theta}\frac{\partial \theta}{\partial \underline{a}}\frac{\partial \underline{a}}{\partial t}ds = \left[\int_0^L T^T \underline{q}\underline{\Phi}^T ds\right]\dot{\underline{a}} \triangleq J\dot{\underline{a}}. \quad (23)$$

Obviously, the Jacobian defined above will have infinitely many columns and clearly does not lend itself to the direct computation of singular values and principal direction vectors as in [9]. However, close inspection of J,

$$J = \begin{bmatrix} -\int s_\theta \Phi_1 ds & -\int s_\theta \Phi_2 ds & \cdots \\ \int c_\theta \Phi_1 ds & \int c_\theta \Phi_2 ds & \cdots \end{bmatrix}, \quad (24)$$

reveals that each element is simply a coefficient in the linear transformation of either s_θ or c_θ. In fact, let us define

$$p_i = \int_0^L \Phi_i(s)sin(\theta)ds, \qquad q_i = \int_0^L \Phi_i(s)cos(\theta)ds \quad (25)$$

and then note that the product JJ^T is

$$JJ^T = \begin{bmatrix} \sum p_i^2 & -\sum p_i q_i \\ -\sum p_i q_i & \sum q_i^2 \end{bmatrix}. \quad (26)$$

Two properties of orthonormal spectral transformations come to our aid now, allowing simplification of the elements of JJ^T,

$$JJ^T = \begin{bmatrix} \int_0^L {s_\theta}^2 ds & -\int_0^L s_\theta c_\theta ds \\ -\int_0^L s_\theta c_\theta ds & \int_0^L {c_\theta}^2 ds \end{bmatrix}. \quad (27)$$

The diagonals reflect the Parseval equality, and the off-diagonals can be easily verified with use of (25) and the orthonormality property of (22).

As with the traditional manipulability ellipsoid, the GME will have principal direction vectors $\underline{v}_i$ with magnitudes λ_i, where $\{\underline{v}_1, \underline{v}_2\}$ and $\{\sqrt{\lambda_1}, \sqrt{\lambda_2}\}$ are the eigenvectors and eigenvalues of JJ^T. Interestingly, the precise choice of spectral decomposition chosen above does not really matter, as long as it adheres to the requirement of orthonormality. Note the intuitive similarity between (27) and the same quantity for the traditional manipulator from earlier, where

$$JJ^T = \begin{bmatrix} \sum_{i=1}^{3} {s_{\theta_i}}^2 & -\sum_{i=1}^{3} c_{\theta_i} s_{\theta_i} \\ -\sum_{i=1}^{3} c_{\theta_i} s_{\theta_i} & \sum_{i=1}^{3} {c_{\theta_i}}^2 \end{bmatrix} \quad (28)$$

Examples of the GME will appear shortly.

5 The Constrained Manipulability Ellipsoid

As mentioned before, the global manipulability ellipsoid derives from the functional norm of $\dot{\theta}$. In a sense, the GME illustrates how the end-effector would move if an infinite number of actuators (or a "distributed" actuator) were specifying the shape of the backbone. In reality, θ is constrained to move only in certain directions dictated by the actuator positions and the physics acting on the backbone; that is, the actuators specify $\{\theta(s_1)...\theta(s_n)\}$. This constraint is captured by a functional mapping from the modal coefficients a_i to the actuator positions,

$$h : \{\theta(s_1)...\theta(s_n)\} \rightarrow \{a_i\}. \quad (29)$$

If we let $\theta(s_1)$ through $\theta(s_n)$ form the elements of the vector $\underline{\theta} \in \Re^n$, we can rewrite the mapping as

$$\underline{a} = h(\underline{\theta}). \quad (30)$$

In general, h is a one-to-many mapping, as there can be an infinitely large set $\{a_i\}$. Because of this, the modal decomposition in the derivation of the GME required the property of orthonormality in order to arrive at a closed-form simplification of the product JJ^T. If, however, a (possibly non-orthogonal) set of basis functions exists for which h is one-to-one or even "finite-to-finite", then no such simplification need be made because a direct calculation of JJ^T is possible.

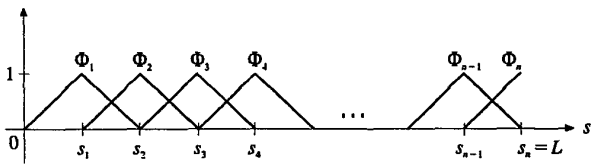

Figure 3: The basis functions $\Phi_i(s)$ as defined in the text.

Under the conditions of small applied end-effector loads, the planar robots of interest in this paper will exhibit piece-wise linear angle functions. In this case, the proper choice of basis functions $\Phi_i(s)$ will permit a one-to-one mapping h. For simplicity, let us assume that the n cable termination points are equally spaced, such that $s_i = \frac{iL}{n}$. Now define

$$\Phi_i(s) = \begin{cases} \frac{n}{L}(s - s_{i-1}) & s_{i-1} < s \leq s_i \\ \frac{n}{L}(s_{i+1} - s) & s_i < s \leq s_{i+1} \\ 0 & otherwise \end{cases}, \quad (31)$$

where $s_0 = 0$ and $s_n = L$ as before. Illustrated in figure 3, the Φ_i clearly do not form an orthonormal set, but where $\theta = \sum_{i=1}^{n} a_i \Phi_i$, there is now a one-to-one correspondence between the modal coefficients and the actuator positions. In fact,

$$a_i = \theta(s_i), \quad (32)$$

remembering that boundary condition (12a) specifies $\theta(0) = 0$.

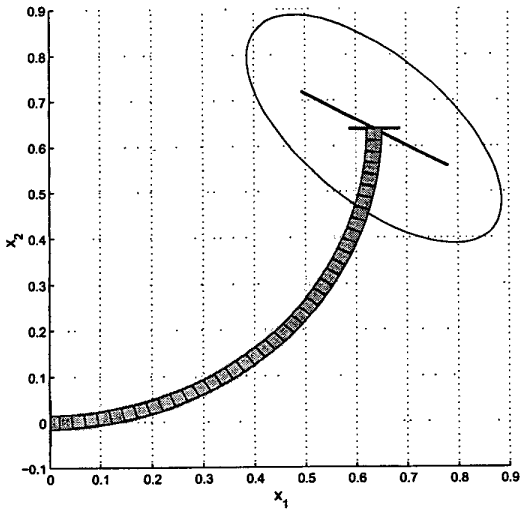

Figure 4: For a 1-section manipulator, the CME indicates a singular configuration (bold line) while the GME does not (thin line).

Now we may again calculate the end-effector velocity,

$$\dot{\underline{x}}(L) = \int_0^L \frac{\partial \underline{q}}{\partial \theta}\frac{\partial \theta}{\partial \underline{a}}\frac{\partial \underline{a}}{\partial \underline{\theta}}\frac{\partial \underline{\theta}}{\partial t}ds = \left[\int_0^L T^T \underline{q}\underline{\Phi}^T ds\right]\frac{\partial \underline{a}}{\partial \underline{\theta}}\dot{\underline{\theta}} \quad (33)$$

Recognizing the modal Jacobian from earlier, and noting that $\frac{\partial \underline{a}}{\partial \underline{\theta}} = I_{n\times n}$, the relationship above is

$$\dot{\underline{x}}(L) = J\dot{\underline{\theta}}. \quad (34)$$

Now we finally come to the definition of the constrained manipulability ellipsoid (CME),

$$CME = \left\{\dot{\underline{x}}(L) : \left\|\dot{\underline{\theta}}\right\| = 1\right\}, \quad (35)$$

which differs only in computation from the traditional ME. As expected, the CME will have principal direction vectors $\{\underline{v}_1, \underline{v}_2\}$ with magnitudes $\left\{\sqrt{\lambda_1}, \sqrt{\lambda_2}\right\}$ where $\underline{v}_i$ and λ_i are the eigenvectors and eigenvalues of the product JJ^T.

Consider figure 4, which illustrates a 1-section manipulator. While the CME reflects the obvious fact that a one actuator manipulator is always singular with respect to a two-dimensional positioning requirement, the GME illustrates that the device as a whole is not in a singular configuration. This is an important distinction, as it highlights two different types of singularities that continuum manipulators can experience: "actuator" singularities, where the robot cannot move in a given direction for lack of actuation, and "configuration" singularities, where the robot cannot move in a given direction under any circumstances. Figure 5 illustrates the GME and CME for a given configuration, giving the robot successively more actuators. Notice that, as the number of actuators increases, the dimensions of the CME approach those of the GME.

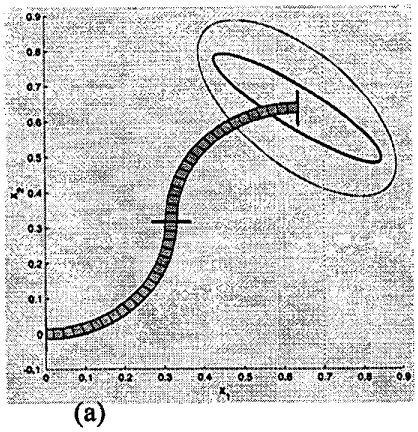

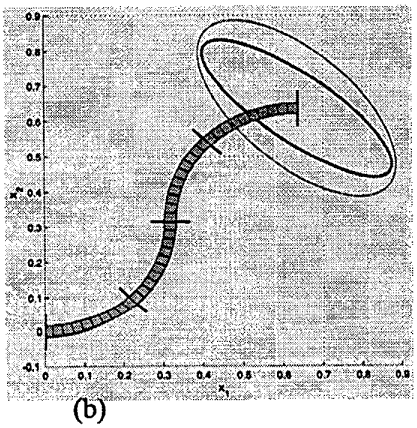

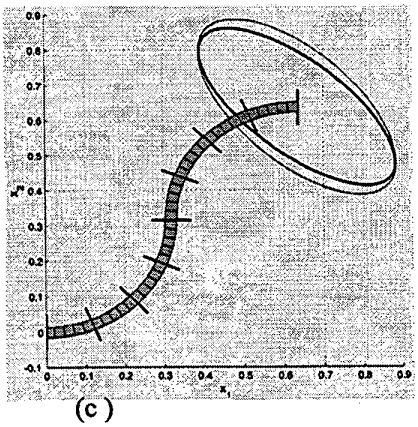

Figure 5: For a given configuration, adding actuators "fills out" the CME (bold line), so that it approaches the dimension of the GME (thin line).

6 The Global Force Ellipsoid

We approach the derivation of the force-torque relationship for a continuum manipulator in much the same way as for traditional manipulators; however, there are a few differences in interpretation. For one, unlike with rigid-link designs, the torques felt at the actuators must necessarily reflect the potential energy of the backbone (i.e. its strain energy or deformation energy). In other words, non-zero moments are required simply to hold the manipulator in a given pose, even with zero applied end-effector force. Consequently, we must speak of the how a differential *change* in applied moments (moment density, actually) Δm results in a change in potential energy.

The principle of virtual work comes to our aid here. Simply stated, "small" arbitrary variations in the potential energy P must balance with variations in the work W applied to (or extracted from) the backbone via the actuators, so that

$$\delta P_a = \delta W_a \quad \text{and} \quad \delta P_b = \delta W_b. \tag{36}$$

P_a and W_a represent the potential energy and applied work for a given moment density m_a with no applied end-effector force. P_b and W_b represent the same quantities for the new moment density m_b required to balance an end-effector force $\underline{f}$. Subtracting the second equality from the first yields

$$\delta(\Delta P) = \delta(\Delta W) \tag{37}$$

On the right hand side, the applied work consists of two components, $\delta(\Delta W_1)$ which reflects the work *exerted by* the system moving the end-effector through a virtual displacement of $\delta\underline{x}(L)$ with a force $\underline{f}$, and $\delta(\Delta W_2)$ which reflects the work *done to* the system by changing the applied moment density. Variations $\delta(\Delta W_1)$ and $\delta(\Delta W_2)$ must have opposite signs, and, since $\underline{f} = \underline{0}$ before the change in moment, $\Delta W_1 = W_1$.

In a rigid-link robot, $\Delta P \equiv 0$, unless one is accounting for gravitational effects, because there is no deformation energy. However, in a continuum robot, changing the applied moment density results in the combination of a change to the net strain energy and the application of an end-effector force (if something exists to "push against"). The relative magnitudes of each of these ingredients will depend on how much the backbone shape changes from before the force is applied to after it is applied. Fortunately, the principle of virtual work does not require that any *actual* work be done, so we can stipulate that the change in moment density induce no change in end-effector position, $\underline{x}(L)$. Consequently, we now make the critical assumption that, if the end-effector forces are small and $\underline{x}(L)$ does not change, then the net change in backbone curvature will be negligibly small. Consequently,

$$\delta(\Delta P) = 0 \tag{38}$$

so

$$\delta(\Delta W) = \delta(\Delta W_2) - \delta(W_1) = 0 \tag{39}$$

and the virtual work must obey

$$\int_0^L \Delta m \delta\theta ds - \underline{f} \cdot \delta\underline{x}(L) = 0 \tag{40}$$

where $\Delta m = m_b - m_a$ is the change in applied moment density. Recall that $\underline{x}' = \underline{q}$, so (40) becomes

$$\int_0^L \Delta m \delta\theta ds = \underline{f}^T \int_0^L T^T \underline{q} \delta\theta ds \tag{41}$$

Because the virtual rotation $\delta\theta$ is arbitrary (to within allowable boundary conditions), the fundamental theory of variational calculus implies that

$$\Delta m = \underline{f}^T T^T \underline{q}. \tag{42}$$

Now we define the global force ellipsoid (GFE) as

$$GFE = \left\{ \underline{f} : \|\Delta m\| = 1 \right\}. \tag{43}$$

Employing relation (42), the GFE requires

$$\|\Delta m\|^2 = \int_0^L (\Delta m)^2 ds = \underline{f}^T \left[T^T \int_0^L \underline{q}\underline{q}^T ds T \right] \underline{f} = 1. \tag{44}$$

This reads in expanded form as

$$\underline{f}^T \begin{bmatrix} \int s_\theta^2 ds & -\int c_\theta s_\theta ds \\ -\int c_\theta s_\theta ds & \int c_\theta^2 ds \end{bmatrix} \underline{f} = 1 \tag{45}$$

which can be seen by reference to (27) as $\underline{f}^T J J^T \underline{f} = 1$. As a result, the GFE will have principal axis vectors of $\{\underline{v}_1, \underline{v}_2\}$ with magnitudes $\left\{ \frac{1}{\sqrt{\lambda_1}}, \frac{1}{\sqrt{\lambda_2}} \right\}$ where $\underline{v}_i$ and λ_i are the eigenvectors and eigenvalues of JJ^T. As with the traditional force and manipulability ellipsoids, the principal axes of the GFE have magnitudes in inverse proportion to those of the GME, while still pointing in the same direction.

7 The Constrained Force Ellipsoid

The crux of the contrast between the GME and CME lies with the observation that it is not possible to access all of the unit-norm angle velocity functions $\dot{\theta}(s)$ with only a finite number of actuators. Similarly, the actuator configuration constrains the applied moment density function $m(s)$ for a practical continuum manipulator. Looking back at the definition of $m(s)$ in (13), we may write m as

$$m(s) = \underline{\eta}(s)^T \underline{\mathcal{I}}. \tag{46}$$

The vector function $\underline{\eta}(s)$ is defined to be a vector of Dirac delta functions,

$$\underline{\eta}(s) = \begin{bmatrix} \delta(s-s_1) & \delta(s-s_2) & \cdots & \delta(s-s_n) \end{bmatrix}^T, \tag{47}$$

not to be confused with the variational operator. Again, we formulate the angle $\theta(s)$ as a weighted sum of basis

functions. Taking the first variation of the end-effector work, we have

$$\begin{aligned}\delta W_1 &= \underline{f}\cdot\delta\underline{x}(L) = \underline{f}\cdot\int_0^L \delta\underline{q}ds \qquad (48)\\ &= \underline{f}^T\int_0^L T^T\underline{q}\delta\theta ds = \underline{f}^T\int_0^L T^T\underline{q}\underline{\Phi}^T\delta\underline{a}ds\\ &= \underline{f}^T\int_0^L T^T\underline{q}\underline{\Phi}^T\frac{\partial\underline{a}}{\partial\underline{\theta}}\delta\underline{\theta}ds\\ &= \underline{f}^T\left[\int_0^L T^T\underline{q}\underline{\Phi}^T ds\right]I_{n\times n}\delta\underline{\theta} = \underline{f}^T J\delta\underline{\theta}.\end{aligned}$$

The first variation of the virtual work applied by the actuators is

$$\begin{aligned}\delta(\Delta W_2) &= \int_0^L \Delta m\delta\theta ds = \left[\int_0^L \Delta m\underline{\Phi}^T ds\right]\frac{\partial\underline{a}}{\partial\underline{\theta}}\delta\underline{\theta} \qquad (49)\\ &= \left[\int_0^L (\Delta\underline{T})^T\underline{\eta}(s)\underline{\Phi}(s)^T ds\right]\delta\underline{\theta}\\ &= (\Delta\underline{T})^T\left[\int_0^L \underline{\eta}(s)\underline{\Phi}(s)^T ds\right]\delta\underline{\theta}.\end{aligned}$$

Expanding the term in the brackets with the help of (31), we find

$$\left[\int_0^L \underline{\eta}(s)\underline{\Phi}(s)^T ds\right] = I_{n\times n}. \qquad (50)$$

So, in the end, the virtual work expression for the planar continuum robot is

$$(\Delta\underline{T})^T\delta\underline{\theta} = \underline{f}^T J\delta\underline{\theta}, \qquad (51)$$

and, because $\delta\underline{\theta}$ is arbitrary within allowable boundary conditions, it follows that

$$\Delta\underline{T} = J^T\underline{f}. \qquad (52)$$

We now define the constrained force ellipsoid (CFE) to be

$$CFE = \left\{\underline{f} : \|\Delta\underline{T}\| = 1\right\}. \qquad (53)$$

As usual, if a norm equals one, then so does its square, so

$$\|\Delta\underline{T}\|^2 = \underline{f}^T JJ^T\underline{f} = 1 \qquad (54)$$

and the CFE will have principal axis vectors $\{\underline{v}_1, \underline{v}_2\}$ with magnitudes $\left\{\frac{1}{\sqrt{\lambda_1}}, \frac{1}{\sqrt{\lambda_2}}\right\}$ where $\underline{v}_i$ and λ_i are the eigenvectors and eigenvalues of JJ^T.

As expected, a manipulator with numerous actuators will have a CFE more closely approximating the GFE than one with few actuators. Figure 6 illustrates this for two manipulators in the same configuration, one with eight actuators and one with only four.

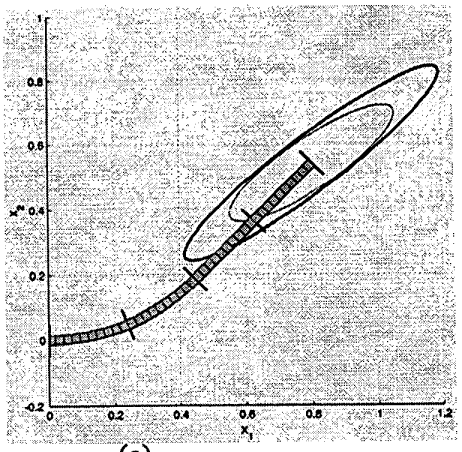

Figure 6: An illustration of the CFE (bold line) and the GFE (thin line) for two manipulators in the same configuration but with differing numbers of actuators.

8 Conclusions

The study of traditional rigid-link robot manipulators has long benefited from the concept of ellipsoids, with the manipulability and force ellipsoids arguably the most prominent. The work in this paper highlights the manipulability and force characteristics of continuum manipulators by introducing four new ellipsoids. Two of these, the global manipulability and force ellipsoids, illustrate the maximum capabilities of a continuum manipulator. The other two, the constrained manipulability and force ellipsoids, take into account the restricted function space accessible by a practical, finitely-actuated continuum robot. We illustrated the intuitive result that the constrained ellipsoids converge to the global ellipsoids as the number of actuators becomes redundant or hyper-redundant. We note that none of the preceding mathematics is restricted

to analyzing what happens at only the end-effector; other locations on the backbone could be just as easily scrutinized.

Several generalizations remain, however. With an appropriate, more thorough, external work expression that accounts for the backbone shear forces exerted by the cables, it might be possible to analyze situations where the shear/axial stiffness is not extremely large, and the backbone is capable of shear and axial deformation in addition to simple bending. Also of interest would be an analysis of the compliance characteristics of the manipulator – the set of all changes to a given backbone location given the application of unit norm forces. It appears that continuum manipulators hold much promise for the future, given a sufficiently rich set of tools to aid in their effective use.

We wish to gratefully acknowledge the following funding agencies for their assistance: NASA (grant NAG5-9785), the NSF-EPSCOR program (grant EPS-9630167) and the South Carolina Space Consortium.

References

[1] I.D. Walker and M.W. Hannan, "A Novel Elephant's Trunk Robot", IEEE/ASME Intl. Conf. on Advanced Intelligent Mechatronics, Atlanta, GA, Sept. 1999, pp. 410-415

[2] I. Gravagne and I.D. Walker, "Kinematic Transformations for Remotely-Actuated Planar Continuum Robots," IEEE Int'l Conf. on Robotics and Automation (ICRA), San Francisco, May 2000, pp.

[3] I. Gravagne and I.D. Walker, "On the Kinematics of Remotely-Actuated Continuum Robots," IEEE Int'l. Conf. on Robotics and Automation (ICRA), San Francisco, May 2000.

[4] I. Gravagne, C.D. Rahn and I.D. Walker, "Good Vibrations: A Vibration Damping Setpoint Controller for Continuum Robots," to appear in the proceedings for the IEEE Int'l Conf. on Robotics and Automation (ICRA), Seoul, Korea, May 2001

[5] I. Gravagne, C.D. Rahn and I.D. Walker, "Large Deflection Dynamics and Control for Planar Continuum Robots," submitted to ASME journal of Dynamic Systems, Measurement and Control.

[6] M. Hannan and I.D. Walker, "Novel Kinematics for Continuum Robots," 7th Int'l Symposium on Advances in Robot Kinematics, Piran, Slovenia, June 2000, pp. 227-238

[7] M. Hannan and I.D. Walker, "Analysis and Initial Experiments for a Novel Elephant's Trunk Robot," Int'l Conf. on Intelligent Robots and System (IROS), Takamatsu, Japan, November 2000, pp. 330-337

[8] G.S. Chirikjian, "Theory and Applications of Hyper-Redundant Robotic Manipulators," Ph.D. thesis, Dept. of Applied Mechanics, California Institute of Technology, June, 1992

[9] T. Yoshikawa, "Manipulability and Redundancy Control of Redundant Mechanisms," Proceedings IEEE Conf. on Robotics and Automation (ICRA), 1985, pp. 1004-1009

[10] G. Robinson and J.B.C. Davies, "Continuum Robots – A State of the Art," Proc. IEEE Int. Conf. Robotics and Automation, Detroit, MI, May 1999, pp. 2849-2854